ADVANCED MATERIALS INTERFACES
Open Access
www.advmatinterfaces.de

# X-Ray and Electron Spectroscopy of the CdS/(Ag,Cu)(In,Ga)$Se_2$ Interface With RbF Treatment

*Dirk Hauschild,* Luisa Both, Mary Blankenship, Constantin Wansorra, Ralph Steininger, Wanli Yang, Dimitrios Hariskos, Wolfram Witte, Rico Gutzler, Michael Powalla, Clemens Heske, and Lothar Weinhardt*

**The chemical and electronic structure of the CdS/(Ag,Cu)(In,Ga)$Se_2$ (CdS/ACIGSe) interface for thin-film solar cells, involving an absorber with a bulk [Ag]/([Ag]+[Cu]) (AAC) ratio of 0.06, a state-of-the-art RbF post-deposition treatment (PDT), and a chemical-bath deposited CdS buffer layer, is studied. To gain a detailed and depth-resolved picture of the CdS/ACIGSe interface, synchrotron- and laboratory-based hard X-ray, soft X-ray, and UV photoelectron spectroscopy, inverse photoemission spectroscopy, and X-ray emission spectroscopy are combined. Compared to the bulk of the absorber, a Cu- and Ga-poor ACIGSe surface is found, with a slightly increased AAC ratio. Strong evidence of a Rb–In–Se species (possibly with some Ag) at the absorber surface is compiled, with a corresponding band gap of 2.79 ± 0.12 eV. This finding is in clear contrast to comparable Ag-free Cu(In,Ga)$Se_2$ absorbers with RbF-PDT. The Rb–In–Se surface species is not removed by the (wet-chemical) CdS deposition process, while some Se diffuses into the CdS layer and segregates at its surface. The CdS buffer layer shows a band gap of 2.48 ± 0.12 eV, and a cliff (≈ −0.4 eV) is determined in the conduction band alignment at the interface between the Rb–In–Se species and the CdS buffer.**

## 1. Introduction

The incorporation of Ag in Cu(In,Ga)$Se_2$ (CIGSe) absorbers for thin-film solar cells, to form (Ag,Cu)(In,Ga)$Se_2$ (ACIGSe) and thus increase the absorber band gap, was suggested 20 years ago.[1] Later, Shafarman et al. processed ACIGSe devices that showed higher efficiencies compared to Ag-free CIGSe devices, which was ascribed to an increase in open-circuit voltage ($V_{OC}$).[2,3] The addition of Ag was found to improve grain growth, allowing for reduced temperatures in the absorber growth process and achieving device performances comparable with Ag-free CIGSe.[4–6]

Similar to CIGSe, alkalis (in particular, Na diffusion from the soda-lime glass substrate) play an important role for ACIGSe absorbers.[2,7,8] For the Ag-free materials class, control of the dosage of additional alkali elements (i.e., K, Rb, and Cs) via a post-deposition treatment (PDT) has led to a significant boost in the efficiency of Cu(In,Ga)(S,Se)$_2$ (CIGSSe)-based thin-film solar cells.[9–12] While the origins of some of the PDT effects are still under discussion,[13] several positive effects were identified, including a reduced bulk recombination rate,[14,15] a changed absorber surface chemistry[16–18] and therefore, decreased interface recombination,[19] and the possibility to reduce the CdS buffer

D. Hauschild, L. Both, M. Blankenship, C. Wansorra, R. Steininger, C. Heske, L. Weinhardt
Institute for Photon Science and Synchrotron Radiation (IPS)
Karlsruhe Institute of Technology (KIT)
Kaiserstraße 12, 76131 Karlsruhe, Germany
E-mail: dirk.hauschild@kit.edu

D. Hauschild, L. Both, M. Blankenship, C. Heske, L. Weinhardt
Institute for Chemical Technology and Polymer Chemistry (ITCP)
Karlsruhe Institute of Technology (KIT)
Kaiserstraße 12, 76131 Karlsruhe, Germany

D. Hauschild, M. Blankenship, C. Wansorra, C. Heske, L. Weinhardt
Department of Chemistry and Biochemistry
University of Nevada
Las Vegas (UNLV)
4505 Maryland Parkway, Las Vegas, NV 89154-4003, USA

W. Yang
Advanced Light Source (ALS)
Lawrence Berkeley National Laboratory
1 Cyclotron Road, Berkeley, CA 94720, United States

D. Hariskos, W. Witte, R. Gutzler, M. Powalla
Zentrum für Sonnenenergie- und Wasserstoff-Forschung
Baden-Württemberg (ZSW)
Meitnerstraße 1, 70563 Stuttgart, Germany

The ORCID identification number(s) for the author(s) of this article can be found under https://doi.org/10.1002/admi.202401002



**DOI: 10.1002/admi.202401002**

layer thickness due to a faster and more dense growth start.[9,20] Among the first effects observed for KF-PDT were a decrease of the copper-content at the CIGSe surface[21] and a shift of the valence band maximum away from the Fermi energy.[22] This was later connected to a K–In–Se surface species, leading to an increased surface band gap.[23,24] However, in other cases, no indication of the formation of such a distinct surface species was found.[17,25] Using the heavy alkali RbF-PDT, the ZSW achieved efficiencies up to 22.6%.[11] For these high-efficiency cells, we found an altered absorber surface chemistry, but no indication for a Rb–In–Se surface species and derived a flat conduction band alignment.[16,26] Other groups report Rb accumulation at the CdS/CIGSe interface[27] and Rb in two distinct chemical environments at the CIGSe surface;[18] both findings could suggest the presence of a Rb–In–Se surface species. We note that many publications interpret the presence of an alkali–In–Se surface species as indicator for a separate $KInSe_2$ or $RbInSe_2$ phase, but so far only *one* direct (and only local) evidence of such a "bulk-like" secondary phase at the buffer/absorber interface has been published.[28] While some reports indicate a Rb–In–Se surface species,[14,18] we did not find such a species at the surface of (Ag-free) ZSW CIGSe absorbers deposited by co-evaporation in well-performing solar cells.[16,25,26,29]

Recently, a new CIGSe solar cell efficiency record of 23.6%[30] was reported by the University of Uppsala with an ACIGSe absorber and a RbF-PDT. This was achieved using a pronounced [Ag]/([Ag]+[Cu]) (AAC) ratio of 0.19 and a [Ga]/([Ga]+[In]) (GGI) ratio profile with a steep increase toward the back-contact ("hockey stick" profile). Rb accumulation at the CdS buffer layer/ACIGSe absorber interface was also found, and the authors suggest the presence of a Rb–In–Se phase.[30] A hard X-ray photoelectron spectroscopy (HAXPES) study on CdS/ACIGSe interfaces after RbF- or CsF-PDTs showed decreased Cu and Ga concentrations and an increased Ag content at the absorber surface. A possible formation of an Ag–In–Se-alkali compound was also considered.[31]

In this paper, we report on a comprehensive study of the chemical and electronic structure of a RbF-treated ACIGSe absorber surface and the CdS/ACIGSe interface in a depth-dependent fashion. For this purpose, we use a powerful combination of laboratory-based X-ray photoelectron spectroscopy (XPS), ultraviolet photoelectron spectroscopy (UPS), and inverse photoemission spectroscopy (IPES), together with synchrotron-based hard and soft X-ray photoelectron spectroscopy (HAXPES and PES) and soft X-ray emission spectroscopy (XES).

## 2. Results

### 2.1. Chemical Structure of the ACIGSe Surface and the CdS/ACIGSe Interface

**Figure 1** shows HAXPES survey spectra ($h\nu$ = 2.1 keV) of the ACIGSe absorber and the CBD-CdS/ACIGSe samples as a function of CBD time. In the spectrum of the ACIGSe absorber, all expected absorber signals are visible. However, the Ag, Ga, and Cu lines (see, e.g., Ag 3d, Ga 2p, and Cu 2p) have very low intensities, suggesting an overall low Cu, Ga, and Ag content at the surface. Nevertheless, the AAC ratio at the surface of 0.12 (± 0.03) is a factor of two larger than the XRF-determined bulk value of 0.06

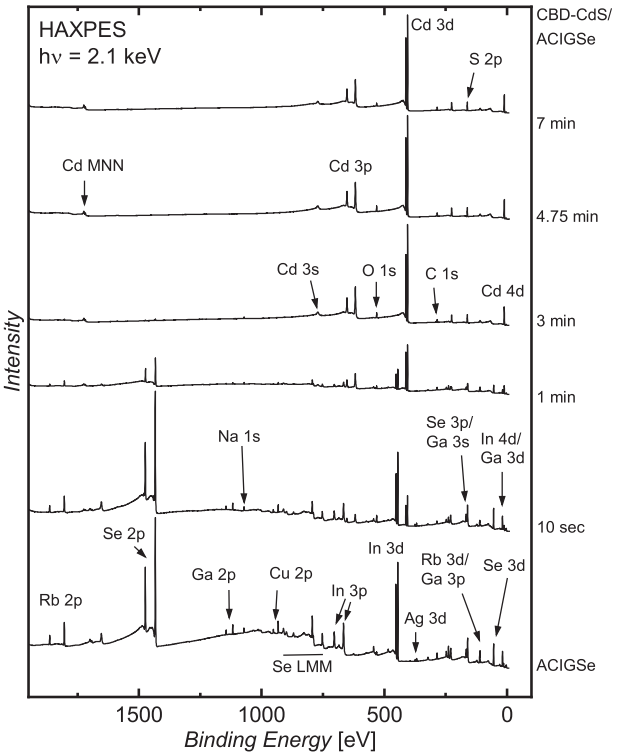


**Figure 1.** HAXPES ($h\nu$ = 2.1 keV) survey spectra of the ACIGSe absorber and CdS/ACIGSe samples with increasing CBD-CdS times. Prominent photoemission and Auger lines are labeled.

(± 0.01). This surface AAC ratio is derived from the Ag 3d and Cu 2p peak areas and by taking photoionization cross-sections, the transmission of the electron analyzer, and the inelastic mean free paths ($\lambda$, IMFP) into account.[32–34] An increased surface AAC ratio was also observed in other ACIGSe studies.[31,35]

Rubidium, deposited during the RbF-PDT, is also found at the surface, most prominently indicated by the Rb $2p_{3/2}$ peak at ≈1804 eV. Compared to other ZSW Ag-free CIGSe absorbers with a GGI of ≈0.3 (see refs. [29,36]), the Rb intensities are significantly larger. We find only trace amounts of F at the surface, which was not entirely removed from the surface by the rinse. We note that the C and O 1s peaks are small for all samples, highlighting that surface contaminations are minimized by avoiding air exposure during sample handling. With increasing CBD time, all absorber-related lines are attenuated, while Cd- and S-related peaks appear and increase in intensity. For CBD-CdS times larger than 3 min, all absorber related lines (except for Se, see discussion of Figure 4) cannot be detected anymore.

To gain a detailed understanding of the impact of the RbF-PDT on the ACIGSe surface, we have investigated the Ag $3d_{5/2}$, Rb 3d/Ga 3p, Se 3d, and In 4d/Ga 3d core levels in a depth-varied picture, as shown in **Figure 2**. To do this, we reduced the exciting photon energy from 2.1 keV to 1000 eV (for Ag 3d and Se 3d) and 400 eV (for Rb 3d/Ga 3p and In 4d/Ga 3d) and therefore increased the surface sensitivity by a factor of 2–3. The characteristic 1/e attenuation length $\lambda$ of the exponentially attenuated photoelectrons changed from ≈3.1 to ≈1.4 nm for Ag 3d, from ≈3.1 to ≈1.9 nm for Se 3d, and from ≈3.5 to ≈1.0 nm for Rb 3d/Ga 3p and In

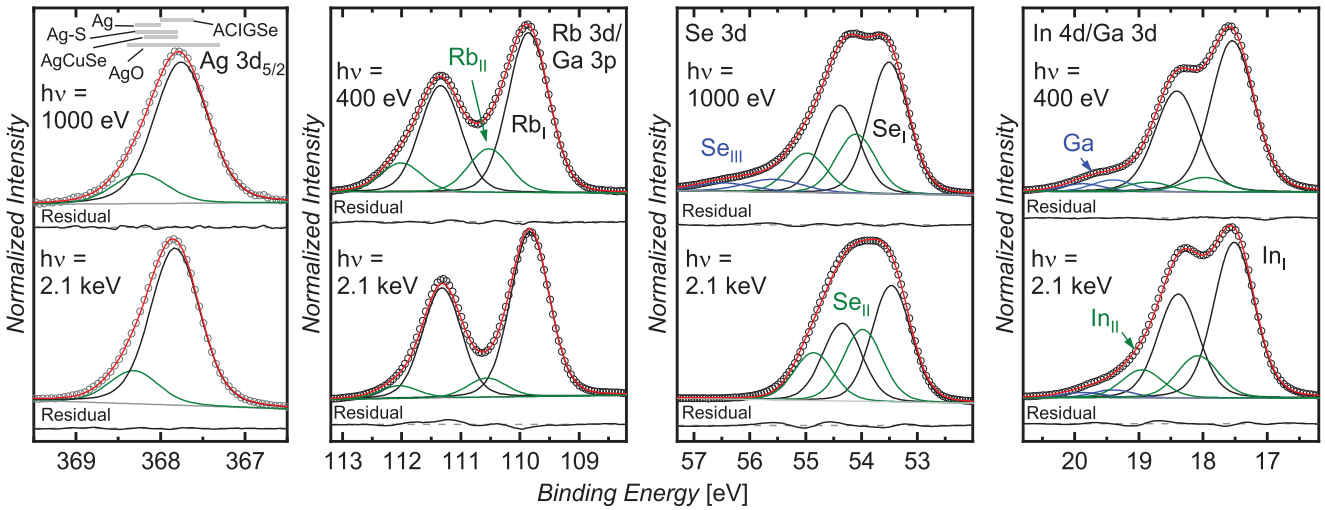


**Figure 2.** PES ($h\nu$ = 400 and 1000 eV, top) and HAXPES ($h\nu$ = 2.1 keV, bottom) spectra: (from left to right) Ag $3d_{5/2}$, Rb 3d/Ga 3p, Se 3d, and In 4d/Ga 3d. Experimental data are depicted as open circles, and the fit sum is depicted as solid red lines. The individual fit components are shown in black, green, and blue (for further details, see text). The residuals are shown below the respective spectra. Literature binding energy ranges for different Ag compounds are given as gray bars above the Ag $3d_{5/2}$ spectrum (top left).[31,37,38]

4d/Ga 3d.[33,34] To extract the different spectral components, we fitted the data of specific regions simultaneously for both excitation energies using a linear background and Voigt profiles. The peak ratios of the spin-orbit doublets were set according to their 2j+1 multiplicity. The Lorentzian and Gaussian widths were kept identical for a given photon energy and core level. In Figure 2, the experimental data is depicted by open circles, the fitted components are plotted in black, green, and blue, and the resulting fit sums are indicated by solid red lines.

To investigate the chemical environment of silver, we analyzed the Ag $3d_{5/2}$ peak as the chemically more sensitive Ag MNN Auger signal is rather weak. The Ag $3d_{5/2}$ peak in Figure 2 shows an asymmetry toward higher binding energies. We thus fit the data with two components, at ≈367.8 and ≈368.3 eV. The peak-area ratio of the two peaks is 0.21 ± 0.02, independent of the excitation energy (within the error bar). The main peak position is in accordance with silver in an ACIGSe environment (Ag $3d_{5/2}$[ACIGSe] = 367.9 ± 0.1 eV).[31] The second, smaller peak could indicate Ag in an oxidic environment or possibly, not fully reacted elemental silver, and/or Ag in an otherwise poorly defined chemical environment.

The Rb 3d/Ga 3p region is dominated by Rb 3d, while contributions of Ga 3p, which would have a larger spin-orbit splitting and lifetime broadening, are negligibly weak. Multiple Rb components must be present because the "dip" between the Rb 3d peaks is less pronounced for the more surface-sensitive measurement ($h\nu$ = 400 eV). The fits give a good description with two Rb 3d components, with Rb $3d_{5/2}$ peaks at ≈109.9 ($Rb_I$, black) and ≈110.5 eV ($Rb_{II}$, green) for both excitation energies. The $Rb_{II}/Rb_I$ intensity ratio increases from 0.11 for 2.1 keV excitation to 0.27 for the more surface-sensitive measurement at 400 eV. For non-rinsed RbF-PDT treated CIGSSe surfaces, two Rb species have been reported before, but the high-binding energy component is typically removed after the rinsing step.[29,39,40] This finding was interpreted as a removal of RbF from the PDT by the rinse: while F was completely removed from the surface, one remaining Rb species was found.[16,41,42] In contrast, Bombsch et al. found two pronounced Rb species after a rinsing step for a CIGSe absorber, for which the low-binding energy component increased for an increased RbF-PDT rate.[18] Due to the absence of any fluorine signal, they assigned the low- ($Rb_I$) and high-binding energy ($Rb_{II}$) species to a Rb–In–Se species and Rb incorporated in the CIGSe absorber, respectively, and argued that the incorporated Rb is homogenously distributed in the CIGSe surface.

To shed light on the ACIGSe surface composition, we determined the Rb: (Ag+Cu): (In+Ga): Se surface stoichiometry to 1.0: 0.2 (±50%): 1.9 (±25%): 3.6 (±25%) and 1.0: 0.4 (±75%): 2.0 (±25%): 3.3 (±25%) for 2.1 keV and 400 eV excitation energy, respectively (taking the cross-section, inelastic mean free path, and analyzer transmission function into account).[32–34] This observation indicates that the Rb content is not significantly changing for the chosen excitation energies and depth sensitivities, suggesting a Rb-containing layer at the surface. Hence, in relation to ref. [18], and as will be discussed throughout the paper, we assign the $Rb_I$ component to a Rb–In–Se surface species. In addition, the increased $Rb_{II}/Rb_I$ ratio for the surface-sensitive measurement ($h\nu$ = 400 eV) suggests that $Rb_{II}$ is present at the outermost absorber surface even after the rinsing procedure. This feature could possibly be related to Rb incorporated in the ACIGSe surface or a slightly oxidized Rb surface species (similar to what has been reported for sodium.[43–45])

To analyze the Se 3d peak, we use the $h\nu$ = 2.1 keV and $h\nu$ = 1000 eV datasets, to avoid the overlapping Ag MNN Auger and Se 3d XPS peaks for the $h\nu$ = 400 eV measurement. Both Se 3d spectra are broad, indicating multiple species. For the spectrum measured with $h\nu$ = 1000 eV excitation energy, additional intensity is found at ≈56 eV binding energy. The fit reveals a minimum of two ($h\nu$ = 2.1 keV) and three ($h\nu$ = 1000 eV) Se 3d components, which is similar to previous studies.[14,18,24] The $Se_{II}$ component (green, Se $3d_{5/2}$ ~54.1 eV) can be ascribed to Se in ACIGSe, and the $Se_I$ component (black, Se $3d_{5/2}$ ≈ 53.5 eV) can be correlated to a Rb–In–Se species. For the measurement

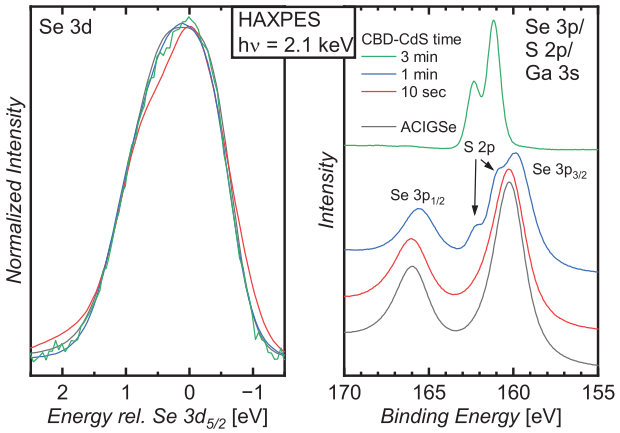


**Figure 3.** Se 3d (left) and Se 3p/S 2p/Ga 3s (right) HAXPES ($h\nu = 2.1$ keV) core-level spectra for increasing CBD-CdS times on the ACIGSe absorber (red, blue, and green). The Se 3d spectra are plotted on one common energy axis, relative to the Se $3d_{5/2}$ position of the absorber (black).

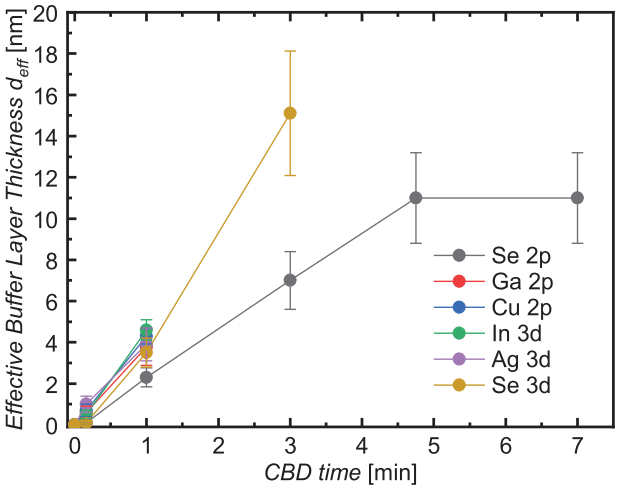


**Figure 4.** Effective CdS buffer layer thickness $d_{\text{eff}} = -\lambda \times \ln(I/I_0)$, as a function of the CBD time derived from peak attenuation of the 2.1 keV data. For the thickest buffer layer, only the Se 2p peak was visible indicating Se diffusion/segregation, similar to Ag-free systems. Profilometer measurements of CBD-CdS films grown on Mo/glass substrates revealed thicknesses of 15, 23, and 50 nm for CBD times of 3, 4.75, and 7 min, respectively.

with increased surface sensitivity, we find that the $Se_I/Se_{II}$ intensity ratio increases by ≈35%, which also suggests that the Rb–In–Se species is present at the surface. In addition, a third component ($Se_{III}$, blue, Se $3d_{5/2} \approx 55.5$ eV) is detected. We attribute this surface component to $Se^0$ and/or to Se in the vicinity of oxygen.[38]

The In 4d/Ga 3d spectra can be fitted with two In-components ($In_I$ [black] and $In_{II}$ [green]) and a small Ga doublet (blue). Taking the In 4d and Ga 3d areas, the photoionization cross-sections, and angular distribution correction into account, the GGI ratio can be calculated.[32,46] While the Ga 3d photoionization cross-section increases by a factor of ≈6 more than that of In 4d when going from 2.1 keV to 400 eV excitation, the Ga 3d/In 4d intensity ratio increases only by a factor of ≈2, indicating a significant decrease of the GGI for the more surface sensitive measurement. In fact, the derived GGIs are 0.11 ± 0.05 and 0.03 ± 0.01 for excitation at 2.1 keV and 400 eV, respectively. With a bulk GGI of 0.31, a significant decrease of the relative Ga-content toward the ACIGSe surface is determined.

The stronger $In_I$ component (black, In $4d_{5/2} \approx 17.5$ eV) can be assigned to a Rb–In–Se species; while, the smaller $In_{II}$ component (green, In $4d_{5/2} \approx 18.1$ eV) is indicative for In in (A)CIGSe. This peak decreases significantly by a factor of ≈3 for the $h\nu$ = 400 eV measurement. Assuming a homogenous Rb–In–Se surface layer, its thickness $d$ can be estimated from the intensities of the ACIGSe components of Se 3d and In 4d measured at $h\nu$ = 400, 1000 eV, and 2.1 keV using the exponential attenuation:

$$I = I_0 \, e^{-d/\lambda} \tag{1}$$

of the PES signal, with $\lambda$ being the IMFP calculated using the QUASES-IMFP code.[33,34] We estimate the thickness to ≈2–5 nm with $\lambda$ = 3 nm ($h\nu$ = 2.1 keV), 1.6 nm ($h\nu$ = 1000 eV), and 1 nm ($h\nu$ = 400 eV),[33,34] respectively.

To investigate the CBD growth start and its impact on the chemical environment of Se, the shape of the Se 3d peak is investigated as a function of CBD time in **Figure 3** (left). For better comparison, the Se 3d spectra are normalized to area and shifted along the ordinate to align the energy relative to the position of the Se $3d_{5/2}$ peak of the absorber. Except for the sample after 10 sec CBD (red), the Se 3d spectra are very similar, indicating similar chemical environments for Se after the initial growth start, i.e., the Rb–In–Se surface layer is not removed by the CBD process. At 10 s CBD-CdS, however, the Se 3d shape shows distinct differences, namely additional intensity at −1 and +2 eV, as well as a different spectral shape around the peak maximum. A similar characteristic is detected for the Se 3p of the 10 s CBD-CdS spectrum in Figure 3 (right), which shows a small broadening toward higher binding energies. For the 10 s CBD-CdS sample, no spectral evidence of sulfur (S 2p ≈161 eV) is detected, while the Cd 3d peaks are clearly visible (see Figure 1). If this Cd would be bound in CdS, a S 2p intensity of ≈½ of that for 1 min CBD (blue, labeled peak doublet) would be expected based on the Cd 3d intensity, photoionization cross-sections,[32] electron analyzer transmission function, and IMFP.[33,34] We ascribe these findings to a complex CBD-CdS growth start, including the formation of Cd—Se bonds, the removal of surface adsorbates, and S/Se intermixing.[20,47–49] For the 3 min CBD data (green), the Se 3p peaks are attenuated and the S 2p peaks clearly visible, which is consistent with the absence of absorber-related lines in Figure 1 for this CBD time.

To further study if Ag in the absorber influences the CdS/ACIGSe interface formation, we analyze the peak area of absorber-related elements as a function of the CBD-CdS time. Assuming a homogenous CdS growth with a layer thickness d (i.e., no diffusion/segregation occurs), an "effective" buffer-layer thickness can be calculated using Equation (1). The results of this analysis, i.e., the effective thickness $d_{\text{eff}} = -\lambda \cdot \ln\left(I/I_0\right)$, is plotted as a function of the CBD time in **Figure 4**. For small CBD times, the effective thickness $d_{\text{eff}}$ determined using different core levels scatter slightly, which can be related to the inhomogeneous CBD-CdS growth start (see discussion

above). The Ag 3d signal attenuation behavior is similar to other absorber-related lines (Ga 2p, Cu 2p, and In 3d), suggesting that no pronounced diffusion of Ag into the CdS layer takes places.

For the 3 min CBD sample, we derive a $d_{eff}$ of 15.1 (± 3.0) nm from the most bulk-sensitive Se 3d signal, which is in good agreement with profilometer measurements on Mo/glass substrates. In contrast, for the surface-sensitive Se 2p signal, a significantly smaller $d_{eff}$ value is determined. For longer CBD times, only the Se 2p lines are detected, while all other absorber peaks are completely attenuated. We interpret this as follows: for the 3 min CBD sample, the bulk-sensitive Se 3d signal mainly originates from Se from the ACIGSe absorber, while the surface-sensitive Se 2p signal exclusively stems from diffused/segregated Se, similar to our study on the Ag-free CdS/CIGSe interface from ZSW[36] and earlier studies of the S-containing CdS/CIGSSe interface.[43–45] For the Ag-free CdS/CIGSe interface from ZSW,[36] we also find a Se 2p-derived $d_{eff}$ of ≈10 nm for the (standard) 7 min CBD-CdS deposition and also find Se at the outermost CdS surface. We thus surmise that a similar process takes place at the CdS/ACIGSe surface.

To further study the chemical environment of the S atoms during the CdS/ACIGSe interface formation, several CBD-CdS/ACIGSe samples are investigated using XES at the S $L_{2,3}$ edge (**Figure 5**). XES is a "photon-in-photon-out" technique with a significantly larger characteristic 1/e attenuation length. For this experiment, the 1/e attenuation length is 110 nm for the incoming and 38 nm for the outgoing photons, respectively.[50] The ACIGSe absorber exhibits a double-structure between 145 and 150 eV, which can be assigned to the Se $M_{2,3}$ emission lines (i.e., transitions from Se 4s-derived states to the spin-orbit-split Se 3p core holes). The sharp peak at 154.5 eV corresponds to the elastic line (3rd harmonic [order] of the undulator [beamline] detected in the 4th order of the spectrometer [206 eV × ¾ = 154.5 eV]). In addition, a broad structure between ≈152 and 157 eV is visible, which we assign to the Ag $M_{4,5}$ emission (in 2nd order of the spectrometer).[50] The low intensity of the Se $M_{2,3}$ signal (note the magnification factor of 200×) originates from the low fluorescence yield, which is ≈two orders of magnitude smaller than for S $L_{2,3}$ emission. The 10 s CdS/ACIGSe sample shows a very similar spectral shape as compared to the ACIGSe absorber, which fits to the above-presented PES results that no S is deposited onto the ACIGSe absorber in the first 10 s of the CBD.

After 3 min CBD-CdS, the spectrum resembles that of the CdS reference, as expected. The two-peak structure between 145 and 150 eV changes its shape, with a maximum at ≈147.5 eV and a shoulder at ≈149 eV; and features at 150.7, 151.8, and ≈156 eV appear. The first two features can be assigned to transitions of the Cd 4d-derived bands into the S $2p_{3/2}$ and S $2p_{1/2}$ core holes, respectively. The separation of 1.2 eV between the two peaks corresponds to the spin-orbit splitting of S 2p. The latter feature is due to transitions from the upper valence band into the S 2p core holes. This "spectral fingerprint" is indicative of S—Cd bonds (as expected for CdS). The 7 min CdS spectrum closely resembles the CdS reference without additional spectral features. In Figure 5, we also show the reference spectrum of $CdSO_4$ as the most-likely S—O bonding environment. The formation of sulfate would emerge as two sharp features at ≈154 and ≈155 eV, accompanied by a broader signal at ≈164 eV.[51] Due to the absence of these features, no indications for the formation of sulfate are detected. In a similar fashion, S—Ag bonds would be represented by the spectral fingerprint of $AgS_2$ with the characteristic upper valence band (≈148 to ≈162 eV). We find no spectral evidence for the formation of S—Ag bonds (possibly due to diffusion of silver into the buffer layer).

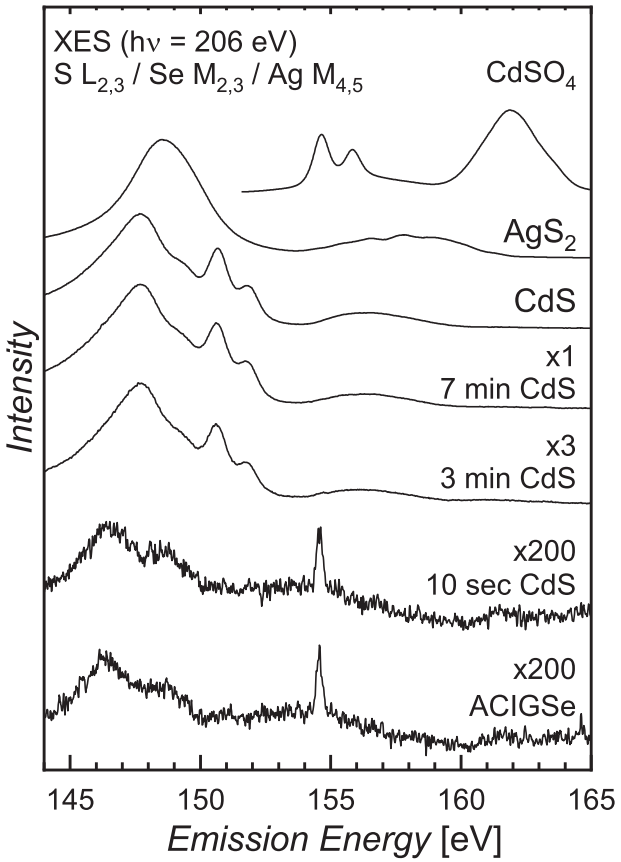


**Figure 5.** S $L_{2,3}$/Se $M_{2,3}$/Ag $M_{4,5}$ XES spectra ($h\nu_{exc.}$ = 206 eV) of the ACIGSe absorber, 10 s, 3 min, and 7 min CBD-CdS/ACIGSe samples. For comparison, the spectra of CdS, $AgS_2$, and $CdSO_4$ references are added and magnification factors are shown on the right.

Summarizing the depth-resolved analysis of the chemical structure of the ACIGSe surface and the CdS/ACIGSe interface, we find a Cu-, Ga-, and Ag-poor ACIGSe surface, with an AAC ratio larger than in the bulk. We find Ag in (at least) two chemical environments, with most of the signal stemming from Ag in ACIGSe. We find a Rb–In–Se surface species, which was not detected for Ag-free CIGSe absorbers from ZSW, despite the fact that they even had a higher RbF dose during the PDT.[16,26,29] This suggests a significant influence of the small Ag addition on the chemical (surface) structure of the absorber. We observe that the Rb–In–Se surface species remains at the buffer/absorber interface after CBD-CdS, potentially leading to a significant impact on the electronic interface structure (see next section). Finally, we find a small degree of Se diffusion/segregation toward the CdS surface, as had been observed for Ag-free CdS/CIGSe interfaces before as well.

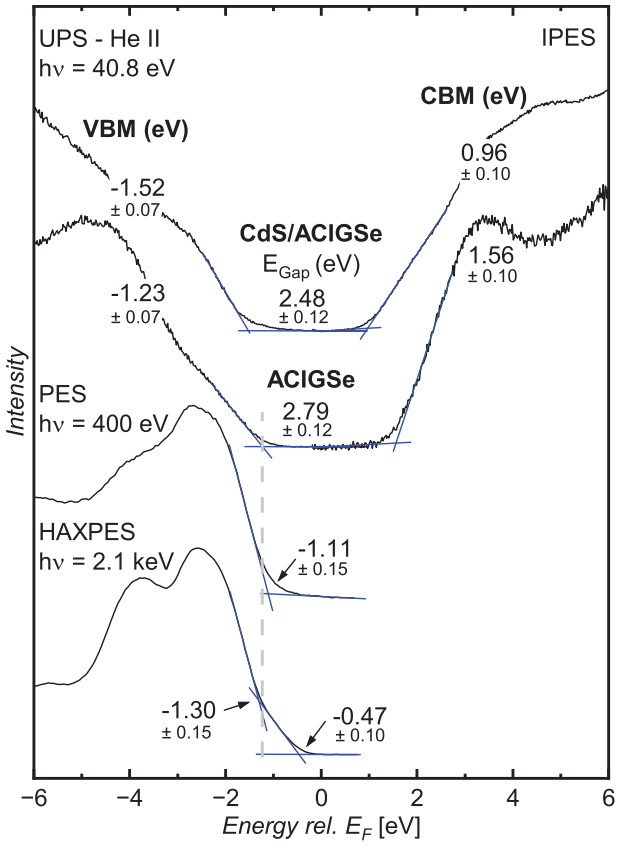


**Figure 6.** (Bottom to top): HAXPES ($h\nu = 2.1$ keV) and PES ($h\nu = 400$ eV) valence band spectra of the ACIGSe surface, as well as UPS (left) and IPES (right) spectra of the $Ar^+$-ion cleaned ACIGSe absorber surface and the 7 min CBD-CdS/ACIGSe sample. The valence band maxima (VBM) and the conduction band minima (CBM) were determined with a linear extrapolation of the leading edges and are listed on the corresponding spectra. The surface band gaps $E_{Gap}$ of the ACIGSe and CdS/ACIGSe samples are given in the center. The vertical gray dashed line indicates the VBM of the surface species. All values are given in eV.

### 2.2. Electronic Structure of the CdS/ACIGSe Interface

In this section, we investigate the electronic structure of the CdS/ACIGSe interface using HAXPES, PES, UPS, and IPES. In particular, we focus on the impact of the Rb–In–Se surface species that remains at the buffer/absorber interface after CBD-CdS. With the three photoemission techniques, we probe the relevant hole transport levels (i.e., a hole at the valence band maximum [VBM]) in a depth-resolved fashion. With IPES, we determine the device-relevant electron transport level (i.e., an electron at the conduction band minimum [CBM]). The VBM and CBM positions are determined using a linear extrapolation of the leading spectral edges.[52] **Figure 6** displays (from bottom to top), the valence band spectra of the ACIGSe absorber excited at 2.1 keV, 400 eV, and 40.8 eV (UPS, He II), the 7 min CBD-CdS/ACIGSe UPS spectrum, and the IPES spectra of the ACIGSe and CdS/ACIGSe samples on the right. For the UPS/IPES measurements, the ACIGSe absorber and the 7 min CdS/ACIGSe sample are treated with 50 eV $Ar^+$-ions for 40 min to remove unwanted surface adsorbates, which is necessary due to the very low IMFP of these techniques.

The linear extrapolation of the leading edge for the ACIGSe UPS spectrum is straight-forward, and we derive a VBM value of $-1.23 \pm 0.07$ eV. At and just above the VBM, the spectrum shows a small tail, which is caused by experimental and lifetime broadening in the measurement. The observed tail is significantly more intense when exciting with 400 eV photons and then even more prominent for the 2.1 keV measurement. In both cases, the tail is significantly larger than the expected broadening; and thus, indicative of real states close to the VBM that are present deeper inside the sample and probed by the photoelectrons at higher excitation energies (and thus higher kinetic energies). We have found similar tails in transparent conductive oxides (e.g., (Zn,Mg)O[53] and ZnO[54]) and a defect-rich $Cu(In,Ga)S_2$ absorber[55] for photoelectrochemical water splitting. In both cases, the tail was attributed to a large number of (surface) defects. As, in the present case, this tail becomes more prominent when looking deeper inside the sample with higher excitation energies, it can rather be attributed to the VBM of the ACIGSe absorber buried below the Rb–In–Se surface layer. In the case of the 2.1 keV measurement, the tail shows a distinct edge, which allows us to separate the VBM of both layers. Hence, we derive values of $-0.47 \pm 0.10$ eV for the tail (i.e., the VBM of ACIGSe) and $-1.30 \pm 0.15$ eV for the main edge (i.e., the VBM of the Rb–In–Se surface layer).

Using the VBM determined with UPS ($-1.23 \pm 0.07$ eV) and the IPES-determined CBM of $1.56 \pm 0.10$, we find a band gap of $2.79 \pm 0.12$ eV for the absorber surface. This is significantly larger than the typical CIGSe surface band gap of 1.4–1.6 eV[26,56,57] and also larger than that of bulk $Ag(In,Ga)Se_2$ (i.e., with a complete replacement of Cu by Ag), which was reported as ≈1.5–1.6 eV.[58] However, our value agrees with a reported bulk band gap of a co-evaporated $RbInSe_2$ (as determined by optical spectroscopy) of 2.8 eV.[59] This results supports our assignment of a Rb–In–Se species at the absorber surface and gives a more direct determination of the electronic band gap and the location of the Fermi energy within the gap.

In a similar fashion, the band edges of the 7 min CdS/ACIGSe sample are determined, resulting in a VBM and CBM of $-1.52 \pm 0.07$ eV and $0.96 \pm 0.10$ eV, respectively. Together, this gives a band gap of $2.48 \pm 0.12$ eV at the CdS surface. This band gap value is in good agreement with other CdS band gap values determined by UPS/IPES,[26,60] as well as optical spectroscopy.[61] Note that the observed diffusion of Se into the CdS buffer layer and to its surface only plays a minor role here, due to the low Se concentration (Se/S ratio is ≈0.002).

In a first direct comparison of the absorber and buffer layers, the CBMs indicate a negative conduction band offset (CBO). For a quantification and correct depiction of the electronic interface structure,R however, additional band bending induced by the interface formation needs to be taken into account.

To determine this correction, the relative shifts of the ACIGSe and CdS core levels are monitored by XPS for the thin CBD-CdS samples. We determine a small, additional downward bending $-0.03 \pm 0.02$ eV for the ACIGSe absorber core levels and $-0.16 \pm 0.04$ eV for the CdS layer core levels. Together with the CBM and VBM values of the ACIGSe absorber and CdS buffer layer, a band diagram is derived as depicted in **Figure 7** (the interface-induced

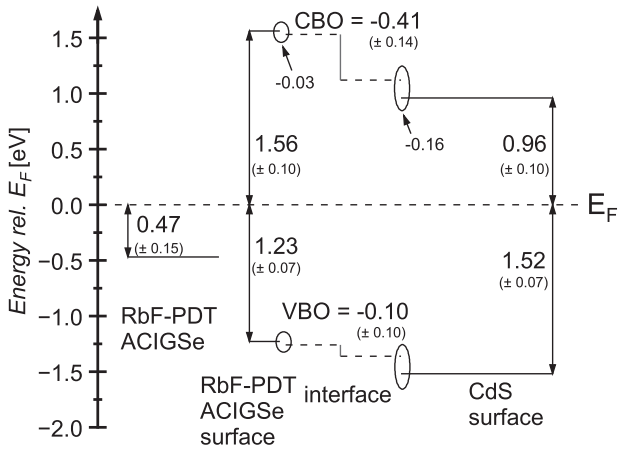


**Figure 7.** Schematic illustration of the band alignment of the CdS/ACIGSe interface with RbF treatment (note that, for a meaningful statement about band offsets at the interface, such alignments must always be presented with respect to the Fermi energy $E_F$, as is done here). The determined band edges are shown for the outermost Rb–In–Se layer (see text), the VBM of the ACIGSe absorber "underneath," and the CdS buffer layer surface. The conduction band and valence band offsets (CBO and VBO, respectively) are refined by the interface-induced band bending. The thin Rb–In–Se layer with a band gap of 2.79 ± 0.12 eV is expected to act as tunneling barrier for charge carriers, reducing interface recombination. All values are given in eV.

band bending corrections are indicated by ovals). We find a negative CBO of −0.41 ± 0.14 eV and a negative valence band offset (VBO) of −0.10 ± 0.10 eV. A cliff in the conduction band is often found for wide-gap absorbers with CdS (e.g., refs. [60,62]); in the presence of strong interface recombination, this is accompanied by a significant $V_{OC}$ loss.[63,64]

For Ag-free ZSW CIGSe absorbers *with* RbF-PDT, in contrast, no Rb–In–Se surface species and a flat conduction band alignment are found.[16,25,26,29] Such flat conduction band alignments are typically derived for well-performing chalcopyrite-based solar cells.[26,57,65] In the present case, the addition of Ag, even at low concentrations (integral AAC ratio of 0.06), induces the formation of the Rb–In–Se surface layer. We speculate that this reduces interface recombination by spatially separating the region of the lowest CBM from that of the highest VBM. Thus, intermediate layers in cliff arrangements could help to improve widegap chalcopyrite-based devices (either with Ag alloying, high GGI, or high S content in CIGSSe).

## 3. Summary

The depth-resolved chemical and electronic structure of a (Ag,Cu)(In,Ga)$Se_2$ (ACIGSe) absorber after RbF post-deposition treatment (PDT) and its interface with a chemical-bath deposited CdS buffer layer is investigated. For a comprehensive picture, lab- and synchrotron-based techniques were combined, including XPS, HAXPES, UPS, IPES, and XES. In comparison to the nominal ACIGSe composition, the absorber surface is copper, gallium, and silver poor. The [Ag]/([Ag]+[Cu]) ratio of 0.12 (± 0.03) at the surface is significantly larger than the integral bulk value of 0.06. We find an ≈2–5 nm thin surface layer that is dominated by a Rb–In–Se species (possibly containing some Ag), which was previously not detected for comparable Ag-free Cu(In,Ga)$Se_2$ absorbers, despite a lower amount of evaporated RbF used for the ACIGSe absorber.[16,26,29] This suggests that the formation of the Rb–In–Se species depends on subtle variations in sample processing—the absorber surface termination is influenced by the entire growth history, rather than just the presence and concentrations of elements provided in the last process steps. The corresponding ACIGSe electronic surface band gap was determined by combining UPS and IPES, yielding a value of 2.79 ± 0.12 eV, similar to literature values of bulk $RbInSe_2$. The Rb–In–Se species remaines at the CdS/ACIGSe interface after chemical-bath deposition of CdS. The band alignment between absorber and CdS buffer, at first sight, indicates an unfavorable cliff-like band alignment of −0.41 ± 0.14 eV. However, we speculate that the thin Rb–In–Se layer spatially separates the band edges, thereby reducing interface recombination. This could be a promising approach toward optimizing other wide-gap chalcopyrite absorbers and their interfaces to suitable buffer materials. Overall, we find that the addition of small amounts of Ag to the ZSW CIGSe absorber *significantly* changes the chemical and electronic structure of the RbF post-deposition-treated ACIGSe absorber surface and the CdS/ACIGSe interface and demonstrate the need for a comprehensive experimental approach to derive the subtleties of such applied and complex interfaces.

## 4. Experimental Section

The ACIGSe solar-cell absorbers were grown at ZSW using the in-line multi-stage co-evaporation process, which is described in detail in ref. [66]. Briefly, Ag, Cu, In, Ga, and Se were co-evaporated onto a sputter-coated Mo/soda-lime glass substrate at elevated temperatures. Ag was introduced during the second stage. After the absorber deposition, a RbF-PDT was performed in a Se atmosphere without breaking the vacuum. In comparison to the RbF-PDT on CIGSe absorbers, a reduced source temperature was used, resulting in ≈25% less RbF at the ACIGSe surface.

Subsequently, the ACIGSe absorbers were rinsed for 60 s in an ammonia solution to remove excess RbF material from the surface. The CdS buffer layer was deposited in a chemical-bath deposition (CBD) step. Both the rinse as well as the CBD process step were carried out with an ammonia concentration of 1.5 M. A CdS thickness series was prepared by stopping the 7-min process (corresponding to ≈50 nm thickness, as determined by profilometer measurements of the same CBD process on a Mo/glass substrate) after different shorter deposition times, i.e., 10 s, 1 min, 3 min, 4.75 min, and 7 min. X-ray fluorescence (XRF) analysis of the ACIGSe absorber revealed integral AAC and GGI ratios of 0.06 and 0.31, respectively, as shown to be optimal in previous ZSW experiments on a large number of samples.[67] Reference cells based on absorbers from the same batch, but with a slightly varied surface treatment (annealing at 200 °C in air for 5 min and a rinse with diluted sodium sulfide), reached a maximum power conversion efficiency (PCE) of 17.2% ($V_{OC}$ = 719 mV, short-circuit current density $J_{SC}$ = 31.23 mA $cm^{-2}$, and fill factor FF = 76.7%) without anti-reflective coating. These cells, with a total area of 0.5 $cm^2$, were processed with a standard 7-min CBD-CdS buffer, 80 nm i-ZnO, and a 250 nm thick Al-doped ZnO front contact (see Supporting Information for JV curves of the best (Ag,Cu)(In,Ga)$Se_2$ thin-film solar cell).

The samples were vacuum-sealed and shipped to the Materials for Energy (MFE) laboratory at KIT. All subsequent sample handling and transport steps were performed without air exposure, using Ar- and $N_2$-filled gloveboxes and sample transfer systems. At KIT, the samples were cut into four sample sets. The first set was transferred directly into the MFE laboratory ultra-high vacuum system for XPS.[68] For this purpose, an Omicron DAR450 twin anode X-ray source (Mg and Al $K_\alpha$) and a monochromatized SIGMA Surface Science MECS x-ray source (Al $K_\alpha$) were utilized

with an Omicron Argus CU electron analyzer. The second sample set was transferred to the X-SPEC beamline[69] at the KIT Light Source for PES and HAXPES using X-SPEC's focusing variable-line-space plane grating monochromator (FVLS-PGM) and the Si(111) double crystal monochromator (DCM), respectively. Spectra were collected with a SPECS Phoibos 225 electron analyzer. For this sample series, photon excitation energies of 400 eV, 1.0 keV, and 2.1 keV were used. The third sample set was shipped to UNLV for XPS, UPS, and IPES measurements. The XPS and UPS data sets were measured with a Scienta R4000 electron analyzer, a SPECS XR 50 dual anode X-ray source, and a Gammadata VUV 5000 monochromatized UV source. The IPES data were collected with a STAIB low-energy electron gun, a UV photon detector using a Semrock HG01-254 mercury line filter, and a Hamamatsu R6834 photomultiplier.[70] The energy axes of all electron spectrometers were calibrated with sputter-cleaned Cu, Ag, and Au references.[38] The exact photon energies for the PES/HAXPES experiments were determined using the kinetic energy of the Au $4f_{7/2}$ peak as a reference.[38] Au and Ag Fermi edges were used to calibrate the energy axis of UPS and IPES, respectively. The fourth sample set was shipped to the ALS for Se $M_{2,3}$/S $L_{2,3}$ XES measurements using the high-transmission X-ray spectrometer[71] of our SALSA endstation[72] at Beamline 8.0.1. The emission energy axis was calibrated using the characteristic features of BN and $CaSO_4$.[51]

## Supporting Information

Supporting Information is available from the Wiley Online Library or from the author.

## Acknowledgements

The authors gratefully acknowledge the financial support from the German Federal Ministry for Economic Affairs and Climate Action (BMWK) under the project "EFFCIS-II" (numbers 03EE1059A and 03EE1059E). D. Hauschild, C. Heske, and L. Weinhardt thank the Deutsche Forschungsgemeinschaft (DFG) for funding of the instrumentation in projects GZ:INST 121384/64-1 FUGG, GZ:INST 121384/65-1 FUGG, and GZ:INST 121384/66-1. This research used resources from the Advanced Light Source, which is a U.S. Department of Energy (DOE) Office of Science User Facility under Contract No. DE-AC02-05CH11231.

Open access funding enabled and organized by Projekt DEAL.

## Conflict of Interest

The authors declare no conflict of interest.

## Data Availability Statement

The data that support the findings of this study are available from the corresponding author upon reasonable request.

## Keywords

(Ag,Cu)(In,Ga)$Se_2$ thin-film solar cells, band alignment, chalcopyrite, chemical structure, electronic structure, RbF post-deposition treatment, Rb–In–Se environment

Received: December 13, 2024
Revised: February 19, 2025
Published online:

[1] T. Nakada, K. Yamada, R. Arai, H. Ishizaki, N. Yamada, *MRS Online Proc. Libr.* **2005**, *865*, 111.
[2] W. Shafarman, C. Thompson, J. Boyle, G. Hanket, P. Erslev, J. D Cohen, in *Proc. 2010 IEEE 35th Photovoltaic Specialists Conf. (PVSC)*, IEEE, Piscataway, NJ **2010**, pp. 325–329.
[3] P. T. Erslev, J. Lee, G. M. Hanket, W. N. Shafarman, J. D. Cohen, *Thin Solid Films* **2011**, *519*, 7296.
[4] L. Chen, J. Lee, W. N. Shafarman, *IEEE J. Photovolt.* **2014**, *4*, 447.
[5] J. H. Boyle, B. E. McCandless, W. N. Shafarman, R. W. Birkmire, *J. Appl. Phys.* **2014**, *115*, 223504.
[6] K. Kim, J. W. Park, J. S. Yoo, J. Cho, H.-D. Lee, J. H. Yun, *Sol. Energy Mater. Sol. Cells* **2016**, *146*, 114.
[7] X. Zhang, M. Kobayashi, *IEEE J. Photovolt.* **2017**, *7*, 1426.
[8] L.-H. Tu, N. T. T. Tran, S.-K. Lin, C.-H. Lai, *Adv. Energy Mater.* **2023**, *13*, 2301227.
[9] A. Chirilă, S. Buecheler, F. Pianezzi, P. Bloesch, C. Gretener, A. R. Uhl, C. Fella, L. Kranz, J. Perrenoud, S. Seyrling, R. Verma, S. Nishiwaki, Y. E. Romanyuk, G. Bilger, A. N. Tiwari, *Nat. Mater.* **2011**, *10*, 857.
[10] P. Jackson, D. Hariskos, R. Wuerz, O. Kiowski, A. Bauer, T. M. Friedlmeier, M. Powalla, *Phys. Status Solidi RRL* **2015**, *9*, 28.
[11] P. Jackson, R. Wuerz, D. Hariskos, E. Lotter, W. Witte, M. Powalla, *Phys. Status Solidi RRL* **2016**, *10*, 583.
[12] M. Nakamura, K. Yamaguchi, Y. Kimoto, Y. Yasaki, T. Kato, H. Sugimoto, *IEEE J. Photovolt.* **2019**, *9*, 1863.
[13] S. Siebentritt, E. Avancini, M. Bär, J. Bombsch, E. Bourgeois, S. Buecheler, R. Carron, C. Castro, S. Duguay, R. Félix, E. Handick, D. Hariskos, V. Havu, P. Jackson, H.-P. Komsa, T. Kunze, M. Malitckaya, R. Menozzi, M. Nesladek, N. Nicoara, M. Puska, M. Raghuwanshi, P. Pareige, S. Sadewasser, G. Sozzi, A. N. Tiwari, S. Ueda, A. Vilalta-Clemente, T. P. Weiss, F. Werner, et al., *Adv. Energy Mater.* **2020**, *10*, 1903752.
[14] T. Kodalle, M. D. Heinemann, D. Greiner, H. A. Yetkin, M. Klupsch, C. Li, P. A. van Aken, I. Lauermann, R. Schlatmann, C. A. Kaufmann, *Sol. RRL* **2018**, *2*, 1800156.
[15] T. Sakurai, N. Ishida, S. Ishizuka, M. M. Islam, A. Kasai, K. Matsubara, K. Sakurai, A. Yamada, K. Akimoto, S. Niki, *Thin Solid Films* **2008**, *516*, 7036.
[16] D. Kreikemeyer-Lorenzo, D. Hauschild, P. Jackson, T. M. Friedlmeier, D. Hariskos, M. Blum, W. Yang, F. Reinert, M. Powalla, C. Heske, L. Weinhardt, *ACS Appl. Mater. Interfaces* **2018**, *10*, 37602.
[17] M. Mezher, L. M. Mansfield, K. Horsley, M. Blum, R. Wieting, L. Weinhardt, K. Ramanathan, C. Heske, *Appl. Phys. Lett.* **2017**, *111*, 071601.
[18] J. Bombsch, E. Avancini, R. Carron, E. Handick, R. Garcia-Diez, C. Hartmann, R. Félix, S. Ueda, R. G. Wilks, M. Bär, *ACS Appl. Mater. Interfaces* **2020**, *12*, 34941.
[19] F. Pianezzi, P. Reinhard, A. Chirilă, B. Bissig, S. Nishiwaki, S. Buecheler, A. N. Tiwari, *Phys. Chem. Chem. Phys.* **2014**, *16*, 8843.
[20] T. M. Friedlmeier, P. Jackson, D. Kreikemeyer-Lorenzo, D. Hauschild, O. Kiowski, D. Hariskos, L. Weinhardt, C. Heske, M. Powalla, in *Proc. 2016 IEEE 43rd Photovoltaic Specialists Conf. (PVSC)*, IEEE, Piscataway, NJ **2016**, pp. 457–461.
[21] A. Chirilă, P. Reinhard, F. Pianezzi, P. Bloesch, A. R. Uhl, C. Fella, L. Kranz, D. Keller, C. Gretener, H. Hagendorfer, D. Jaeger, R. Erni, S. Nishiwaki, S. Buecheler, A. N. Tiwari, *Nat. Mater.* **2013**, *12*, 1107.
[22] P. Pistor, D. Greiner, C. A. Kaufmann, S. Brunken, M. Gorgoi, A. Steigert, W. Calvet, I. Lauermann, R. Klenk, T. Unold, M.-C. Lux-Steiner, *Appl. Phys. Lett.* **2014**, *105*, 063901.
[23] E. Handick, P. Reinhard, J.-H. Alsmeier, L. Köhler, F. Pianezzi, S. Krause, M. Gorgoi, E. Ikenaga, N. Koch, R. G. Wilks, S. Buecheler, A. N. Tiwari, M. Bär, *ACS Appl. Mater. Interfaces* **2015**, *7*, 27414.
[24] E. Handick, P. Reinhard, R. G. Wilks, F. Pianezzi, T. Kunze, D. Kreikemeyer-Lorenzo, L. Weinhardt, M. Blum, W. Yang, M. Gorgoi, E. Ikenaga, D. Gerlach, S. Ueda, Y. Yamashita, T. Chikyow, C. Heske, S. Buecheler, A. N. Tiwari, M. Bär, *ACS Appl. Mater. Interfaces* **2017**, *9*, 3581.

[25] A. Eslam, R. Wuerz, D. Hauschild, L. Weinhardt, W. Hempel, M. Powalla, C. Heske, *Thin Solid Films* **2021**, *739*, 138979.
[26] D. Hauschild, D. Kreikemeyer-Lorenzo, P. Jackson, T. M. Friedlmeier, D. Hariskos, F. Reinert, M. Powalla, C. Heske, L. Weinhardt, *ACS Energy Lett.* **2017**, *2*, 2383.
[27] M. Raghuwanshi, A. Vilalta-Clemente, C. Castro, S. Duguay, E. Cadel, P. Jackson, D. Hariskos, W. Witte, P. Pareige, *Nano Energy* **2019**, *60*, 103.
[28] N. Taguchi, S. Tanaka, S. Ishizuka, *Appl. Phys. Lett.* **2018**, *113*, 113903.
[29] E. Pyatenko, D. Hauschild, V. Mikhnych, R. Edla, R. Steininger, D. Hariskos, W. Witte, M. Powalla, C. Heske, L. Weinhardt, *ACS Appl. Mater. Interfaces* **2023**, *15*, 53113.
[30] J. Keller, K. Kiselman, O. Donzel-Gargand, N. M. Martin, M. Babucci, O. Lundberg, E. Wallin, L. Stolt, M. Edoff, *Nat. Energy* **2024**, *9*, 467.
[31] N. M. Martin, T. Törndahl, E. Wallin, K. A. Simonov, H. Rensmo, C. Platzer-Björkman, *ACS Appl. Energy Mater.* **2022**, *5*, 461.
[32] M. B. Trzhaskovskaya, V. I. Nefedov, V. G. Yarzhemsky, *At. Data Nucl. Data Tables* **2001**, *77*, 97.
[33] S. Tanuma, C. J. Powell, D. R. Penn, *Surf. Interface Anal.* **1994**, *21*, 165.
[34] S. Tougaard, "QUASES (QUantitative Analysis of Surfaces by Electron Spectroscopy)", http://www.quases.com/home/ (accessed: December 2024).
[35] T. Helder, A. Kanevce, M. Zinßer, R. Gutzler, S. Paetel, W. Hempel, T. Magorian Friedlmeier, M. Powalla, *Prog. Photovolt.: Res. Appl.* **2023**, *31*, 1205.
[36] D. Hauschild, R. Steininger, D. Hariskos, W. Witte, S. Tougaard, C. Heske, L. Weinhardt, *J. Vac. Sci. Technol., A* **2021**, *39*, 063216.
[37] A. Naumkin, A. Kraut-Vass, S. Gaarenstroom, C. Powell, "NIST X-ray Photoelectron Spectroscopy (XPS) Database, Version 5.0," http://srdata.nist.gov/xps/Default.aspx, **2024**.
[38] J. F. Moulder, W. F. Stickle, P. E. Sobol, K. D. Bomben, *Handbook of X-Ray Photoelectron Spectroscopy*, Perkin-Elmer Corporation, Shelton, CT **1992**.
[39] C. K. Boumenou, H. Phirke, J. Rommelfangen, J.-N. Audinot, S. Nishiwaki, T. Wirtz, R. Carron, A. Redinger, *Adv. Funct. Mater.* **2023**, *33*, 2300590.
[40] N. Maticiuc, T. Kodalle, J. Lauche, R. Wenisch, T. Bertram, C. A. Kaufmann, I. Lauermann, *Thin Solid Films* **2018**, *665*, 143.
[41] P. Tsoulka, S. Harel, L. Arzel, A. Weber, T. Niesen, P. Reyes-Figueroa, H. Elanzeery, T. Dalibor, N. Barreau, *Appl. Surf. Sci.* **2023**, *614*, 155830.
[42] A. Elizabeth, S. K. Sahoo, H. Phirke, T. Kodalle, T. D. Kühne, J.-N. Audinot, T. Wirtz, A. Redinger, C. A. Kaufmann, H. Mirhosseini, H. Mönig, *ACS Appl. Mater. Interfaces* **2022**, *14*, 34101.
[43] C. Heske, R. Fink, E. Umbach, W. Riedl, F. Karg, *Appl. Phys. Lett.* **1996**, *68*, 3431.
[44] C. Heske, G. Richter, Z. Chen, R. Fink, E. Umbach, W. Riedl, F. Karg, *J. Appl. Phys.* **1997**, *82*, 2411.
[45] D. Hauschild, F. Meyer, S. Pohlner, R. Lechner, R. Dietmüller, J. Palm, C. Heske, L. Weinhardt, F. Reinert, *J. Appl. Phys.* **2014**, *115*, 183707.
[46] C. Wansorra, D. Hauschild, R. Steininger, C. Heske, L. Weinhardt, *in preparation.* **2025**.
[47] C. Heske, D. Eich, R. Fink, E. Umbach, T. van Buuren, C. Bostedt, L. J. Terminello, S. Kakar, M. M. Grush, T. A. Callcott, F. J. Himpsel, D. L. Ederer, R. C. C. Perera, W. Riedl, F. Karg, *Appl. Phys. Lett.* **1999**, *74*, 1451.
[48] L. Weinhardt, T. Gleim, O. Fuchs, C. Heske, E. Umbach, M. Bär, H.-J. Muffler, Ch.-H. Fischer, M. C. Lux-Steiner, Y. Zubavichus, T. P. Niesen, F. Karg, *Appl. Phys. Lett.* **2003**, *82*, 571.
[49] L. Weinhardt, M. Bär, S. Pookpanratana, M. Morkel, T. P. Niesen, F. Karg, K. Ramanathan, M. A. Contreras, R. Noufi, E. Umbach, C. Heske, *Appl. Phys. Lett.* **2010**, *96*, 182102.
[50] A. Thompson, J. Kirz, D. Attwood, E. Gullikson, M. Howells, J. Kortright, Y. Liu, A. Robinson, *X-Ray Data Booklet* **2009**.
[51] L. Weinhardt, D. Hauschild, R. Steininger, N. Jiang, M. Blum, W. Yang, C. Heske, *Anal. Chem.* **2021**, *93*, 8300.
[52] T. Gleim, C. Heske, E. Umbach, C. Schumacher, S. Gundel, W. Faschinger, A. Fleszar, C. Ammon, M. Probst, H.-P. Steinrück, *Surf. Sci.* **2003**, *531*, 77.
[53] D. A. Duncan, R. Mendelsberg, M. Mezher, K. Horsley, S. G. Rosenberg, M. Blum, G. Xiong, L. Weinhardt, M. Gloeckler, C. Heske, *Adv. Mater. Interfaces* **2016**, *3*, 1600418.
[54] L. Weinhardt, C. Heske, E. Umbach, T. P. Niesen, S. Visbeck, F. Karg, *Appl. Phys. Lett.* **2004**, *84*, 3175.
[55] J. C. Carter, D. Hauschild, L. Weinhardt, K. Horsley, D. Hariskos, N. Gaillard, C. Heske, *J. Phys. Chem. C* **2023**, *127*, 8235.
[56] D. Hauschild, E. Handick, S. Göhl-Gusenleitner, F. Meyer, H. Schwab, A. Benkert, S. Pohlner, J. Palm, S. Tougaard, C. Heske, L. Weinhardt, F. Reinert, *ACS Appl. Mater. Interfaces* **2016**, *8*, 21101.
[57] M. Morkel, L. Weinhardt, B. Lohmüller, C. Heske, E. Umbach, W. Riedl, S. Zweigart, F. Karg, *Appl. Phys. Lett.* **2001**, *79*, 4482.
[58] J. Kruip, I. Kardosh, T. Köhler, Y. Gao, M. Schmid, *Processes* **2023**, *11*, 392.
[59] T. Kodalle, R. Kormath Madam Raghupathy, T. Bertram, N. Maticiuc, H. A. Yetkin, R. Gunder, R. Schlatmann, T. D. Kühne, C. A. Kaufmann, H. Mirhosseini, *Phys. Status Solidi RRL* **2019**, *13*, 1800564.
[60] M. Blankenship, D. Hauschild, L. Both, E. Pyatenko, W. Witte, D. Hariskos, S. Paetel, M. Powalla, L. Weinhardt, C. Heske, *J. Phys. Chem. C* **2024**, *128*, 339.
[61] U. Roessler, Ed., Landolt-Börnstein - Group III Condensed Matter, *New Data and Updates for II-VI Compounds*, Springer, Berlin Heidelberg, Berlin, Heidelberg, **2009**.
[62] L. Weinhardt, O. Fuchs, D. Groß, G. Storch, E. Umbach, N. G. Dhere, A. A. Kadam, S. S. Kulkarni, C. Heske, *Appl. Phys. Lett.* **2005**, *86*, 062109.
[63] I. Hengel, A. Neisser, R. Klenk, M. C. Lux-Steiner, *Thin Solid Films* **2000**, *361-362*, 458.
[64] R. Klenk, *Thin Solid Films* **2001**, *387*, 135.
[65] D. Hauschild, M. Blankenship, A. Hua, R. Steininger, P. Eraerds, T. Niesen, T. Dalibor, W. Yang, C. Heske, L. Weinhardt, *Sol. RRL* **2023**, *7*, 2201091.
[66] R. Gutzler, W. Witte, A. Kanevce, D. Hariskos, S. Paetel, *Prog. Photovolt.: Res. Appl.* **2023**, *31*, 1023.
[67] S. Essig, S. Paetel, T. M. Friedlmeier, M. Powalla, *JPhys Mater.* **2021**, *4*, 024003.
[68] L. Weinhardt, D. Hauschild, C. Heske, *Adv. Mater.* **2019**, *31*, 1806660.
[69] L. Weinhardt, R. Steininger, D. Kreikemeyer-Lorenzo, S. Mangold, D. Hauschild, D. Batchelor, T. Spangenberg, C. Heske, *J. Synchrotron Radiat.* **2021**, *28*, 609.
[70] H. Yoshida, *Chem. Phys. Lett.* **2012**, *539-540*, 180.
[71] O. Fuchs, L. Weinhardt, M. Blum, M. Weigand, E. Umbach, M. Bär, C. Heske, J. Denlinger, Y.-D. Chuang, W. McKinney, Z. Hussain, E. Gullikson, M. Jones, P. Batson, B. Nelles, R. Follath, *Rev. Sci. Instrum.* **2009**, *80*, 063103.
[72] M. Blum, L. Weinhardt, O. Fuchs, M. Bär, Y. Zhang, M. Weigand, S. Krause, S. Pookpanratana, T. Hofmann, W. Yang, J. D. Denlinger, E. Umbach, C. Heske, *Rev. Sci. Instrum.* **2009**, *80*, 123102.